Infrared fixed point of the SU(3) gauge theory with $N_f = 10$ flavors

Anna Hasenfratz,[1] Ethan T. Neil,[1] Yigal Shamir,[2] Benjamin Svetitsky,[2] and Oliver Witzel[3]

[1] *Department of Physics, University of Colorado, Boulder, CO 80309, USA*
[2] *Raymond and Beverly Sackler School of Physics and Astronomy, Tel Aviv University, 69978 Tel Aviv, Israel*
[3] *Center for Particle Physics Siegen, Theoretische Physik 1, Naturwissenschaftlich-Technische Fakultät, Universität Siegen, 57068 Siegen, Germany*

We use lattice simulations and the continuous renormalization-group method, based on the gradient flow, to calculate the β function and anomalous dimensions of the SU(3) gauge theory with $N_f = 10$ flavors of fermions in the fundamental representation. We employ several improvements to extend the range of available renormalized couplings, including the addition of heavy Pauli-Villars bosons to reduce cutoff effects and the combination of a range of gradient flow transformations. While in the weak coupling regime our result is consistent with those of earlier studies, our techniques allow us to study the system at much stronger couplings than previously possible. We find that the renormalization group β function develops a zero, corresponding to an infrared-stable fixed point, at gradient-flow coupling $g^2 = 15.0(5)$. We also determine the mass and tensor anomalous dimensions: At the fixed point we find $\gamma_m \simeq 0.6$, suggesting that this system might be deep inside the conformal window.

I. INTRODUCTION

The SU(3) gauge theory with ten Dirac fermions in the fundamental representation is the subject of continuing debate. The question is whether its infrared physics is confining or conformal, as determined by the absence or presence of an infrared fixed point (IRFP). The system has been studied by several groups, both with domain wall [1–5] and staggered fermions [6–8]. All these studies have used the finite-volume gradient flow (GF) scheme with a step-scaling renormalization-group transformation [9–11]. While the results are in reasonable agreement at weak gauge couplings, they differ at stronger couplings and reach differing conclusions.

Using domain-wall fermions, Chiu [1, 2] first claimed an IRFP at $g^2 \simeq 7$. His later study [3], however, gave a more cautious assessment. Hasenfratz, Rebbi, and Witzel [4, 5] observed a step-scaling β function that increases in absolute value up to $g^2 \simeq 9$, where it appears to turn towards the abscissa and thus hints at an IRFP at some $g^2 \gtrsim 11$; these simulations were limited by a first-order phase transition blocking access to the $g^2 > 11$ regime. Staggered-fermion calculations by the LatHC collaboration [6–8] studied this system in larger volumes, reaching couplings up to $g^2 \simeq 10$. In this range their β function increases steadily in magnitude and remains in 2σ agreement with the result reported in Refs. [4, 5]. It does not, however, show any sign of a developing IRFP. No definitive conclusion on the infrared behavior of the $N_f = 10$ model has been reached so far.

All the studies listed above were carried out in a range of renormalized coupling limited by large cutoff effects. Recently we have proposed adding heavy Pauli-Villars (PV) bosons to remove ultraviolet fluctuations caused by the many fermion fields [14]. The masses of the PV bosons are kept at the cutoff scale. Thus they decouple in the continuum limit but they do generate a local effective gauge action with well-regularized short-distance properties. We have applied PV improvement successfully in the SU(3) gauge theory with $N_f = 12$ [14] and $N_f = 8$ [15] staggered fermions in the fundamental representation, as well as in a multirepresentation SU(4) gauge theory with Wilson fermions [16]. In all cases we found that the PV improved actions indeed reduced short-distance fluctuations and allowed investigations at stronger renormalized couplings.

In Ref. [16] we applied the continuous β function (CBF) method [17, 18] and uncovered an IRFP at strong coupling. Going beyond the use of PV bosons, we further extended the coupling range by combining the results of a number of lattice gradient flows that possess a common continuum limit. Here we apply the techniques used in

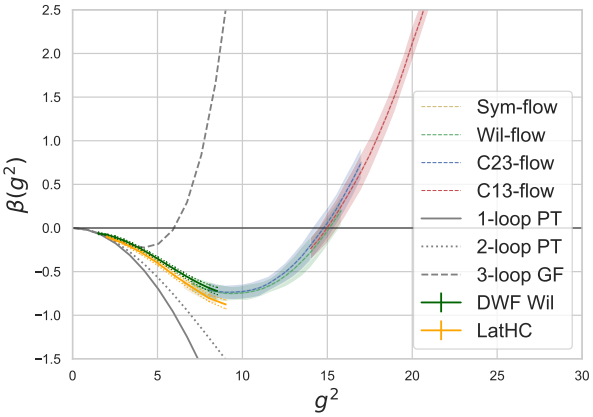

FIG. 1. The β function obtained with four different gradient-flow transformations in overlapping regions. The orange and dark green solid lines, with errors indicated by the dotted lines, are results from staggered and DWF simulations [4–8, 12]. Black solid, dotted and dashed curves correspond to the universal 1- and 2-loop and the gradient flow 3-loop perturbative results [13].

[16] to the SU(3) gauge theory with $N_f = 10$ fundamental flavors, simulated using Wilson fermions. The presence of heavy PV bosons permits study of the system at much stronger renormalized couplings than previously possible. When the CBF method is extended by varying the GF transformation, the accessible range of renormalized coupling is yet larger. We summarize our main result—the β function of the theory—in Fig. 1. By combining overlapping results from different gradient flows, we cover the range $6.5 \lesssim g^2 \lesssim 23$. At weak coupling our prediction is consistent with that of LatHC [7, 8] and overlaps with an CBF result [12] obtained by reanalyzing the Möbius DWF data from Refs. [4, 5] (labeled "DWF Wil" in the figure).[1] Our β function turns around at $g^2 \simeq 10.0$, confirming the hint of an IRFP reported in [5]. At stronger coupling, the β function rises steadily and crosses zero at an IRFP at $g^2_{\rm FP} = 15.0(5)$, implying the theory is infrared conformal.

This paper is organized as follows. In Sec. II we briefly describe the numerical simulations and define the gradient flow transformations. In the following sections we show how we obtain our results and extrapolate them to the infinite-volume and continuum limits. For the β function see Sec. III and for anomalous dimensions of fermion bilinears see Sec. IV. With the exception of the volume extrapolation, the techniques used have been explained at length in our recent paper [16] and hence our presentation here is brief. We discuss our results further in Sec. V.

II. SIMULATION AND GRADIENT FLOW

Our data emerge from four-dimensional configurations of the Euclidean gauge theory, generated by hybrid Monte Carlo simulations of the lattice theory. Our lattice action couples the gauge field to Wilson-clover fermions after smearing the links with normalized hypercubic (nHYP) smearing [19, 20]. The clover coefficient is $c_{SW} = 1$ [21, 22] and the smearing parameters α_i are the original set (0.75, 0.6, 0.3). The plaquette gauge action is supplemented by a term for nHYP dislocation suppression (NDS) [23]. To further tame gauge field roughness, we add 30 Pauli-Villars (bosonic Dirac) fields—three for each fermion flavor—with bare mass $am_{PV} = 1$ [14]. For each lattice coupling β_0 we set the hopping parameter $\kappa \simeq \kappa_c$ so that the fermion mass, calculated from the axial Ward identity, is bounded by $|am_f| < 5 \times 10^{-4}$. The ensembles are listed in Table 1. In the chiral limit the topology is expected to be frozen at $Q = 0$; we monitor the topological charge and confirm this expectation.

We extract the β function and anomalous dimensions using a continuous RG transformation based on gradient flow [8, 16–18, 24–27]. The RG length scale is given by $\sqrt{t}$ where t is the GF time [9]. In continuum language, the GF running coupling at scale $\sqrt{t}$ is defined as

$$g^2 = \frac{\mathcal{N}}{(1+\delta)} t^2 \langle E(t) \rangle \ , \tag{2.1}$$

with the energy density $E = \frac{1}{4} G^a_{\mu\nu} G^a_{\mu\nu}$, calculated from the flowed gauge field strength $G^a_{\mu\nu}$. The constant $\mathcal{N} = 128\pi^2/(3(N_c^2-1))$ is a normalization factor to match to the 1-loop $\overline{\rm MS}$ result, while δ is a small finite-volume correction [11]. The average in Eq. (2.1) is over the ensemble of configurations generated at given lattice coupling β_0. We have estimated the autocorrelation time of our measurements by binning $g^2(t)$ at the maximum flow time used in our analysis; we bin all data in blocks of three in our final analysis to account for the longest autocorrelations found.

The β function is simply

$$\beta(g^2) = -t \frac{\partial g^2}{\partial t} \ . \tag{2.2}$$

The anomalous dimensions (see below) are determined from the derivative of flowed correlation functions of the fermion fields [16, 24, 28].

In the lattice theory, the GF transformation can be performed with different flows, each originating in a particular discretization of the gauge action. We make use of four such lattice flows, corresponding to combinations of plaquette and rectangle terms with coefficients c_p and c_r. Imposing the perturbative normalization $c_p + 8c_r = 1$, we define the Symanzik flow ($c_p = 5/3$), the Wilson flow ($c_p = 1$), and flows called C23 ($c_p = 2/3$) and C13 ($c_p = 1/3$) [16]. The different flows correspond to different renormalized trajectories (RT) of the RG transformation. Ideally, we would choose the RG transformation whose RT is closest to the simulation action. We find that GF with smaller c_p values are better for this purpose at stronger gauge coupling.

Besides this, the energy operator $E(t)$ can be defined by a variety of discretizations. We calculate the W (Wilson), S (Symanzik), and C (clover) operators in order to gauge the approach of each to the continuum limit. The S operator gives the smoothest approach, and so we will focus on results obtained using this operator.

β_0	κ	$L/a = 24$	$L/a = 28$
6.0	0.12742	135	100
6.2	0.12695	100	100
6.3	0.12677	150	100
6.5	0.1265	155	100
6.7	0.1263	135	90
7.0	0.12612	160	110

TABLE 1. List of the ensembles, showing the lattice coupling constant β_0, the hopping parameter κ, and the number of configurations with volume $L^3 \times (2L)$ for the two volumes.

[1] We have obtained the LatHC result from Fig. 10 of Ref. [8], the most recent publication showing the continuous β function obtained by the collaboration.

III. THE β FUNCTION

Raw data for the flowed coupling g^2 and its derivative $\beta(g^2)$ from Wilson and C13 flows, are shown for all ensembles in Fig. 2. One sees an upward flow with increasing t, ever faster for ensembles with larger coupling g^2. The C13 flow has the shortest paths as t grows, indicating that its RT is closest. Moreover, while both flows show that the β function approaches the axis for large g^2, the C13 flow actually shows a positive β function at the strongest coupling, even before taking the continuum limit. This is the first hint of an IRFP. Finally, the figure allows comparison of lattice sizes $L^3 \times (2L)$ for $L/a = 24$ and $L/a = 28$, whence it is seen that differences are very small but not zero.

We determine the continuous β function via the following four steps, ultimately carrying out the limits $L \to \infty$ and $a \to 0$ [18, 27].

A. Infinite volume limit

We take the infinite volume limit, for both g^2 and $\beta(g^2)$, at each bare coupling β_0 and at selected flow times. Finite-size scaling implies that the leading volume dependence of the renormalized GF coupling is $\propto t^2/L^4$.[2] Higher order corrections can hence be suppressed by choosing t/L^2 sufficiently small. In this study we consider two volumes, $L/a = 24$ and 28, and restrict the flow time to $2.8 \leq t/a^2 \leq 3.8$. With this restriction the finite volume effects are well controlled in all ensembles as can be seen already in Fig. 2. In Fig. 3 we plot $\beta(g^4)/g^4$, derived from Wilson flow at fixed flow time $t/a^2 = 3.8$, at all six bare coupling values (see Table 1) and both volumes. The plot also shows the infinite volume extrapolation, assuming the leading order volume dependence is $1/L^4$. The colored bands show quadratic interpolations of the data, which furnish values of $\beta(g^2)$ at intermediate values of g^2 (see below).

In the next two steps we consider mainly the infinite-volume extrapolations. For a cross-check, we show in Fig. 4 the approach of our final β function to infinite volume by plotting directly the results of separately analyzing only $L/a = 24$ or $L/a = 28$. Comparison with Fig. 1 shows that our results, particularly the existence and location of the fixed point $\beta(g^2) = 0$, are essentially independent of lattice volume.

B. Interpolation

In order to take the the continuum limit of $\beta(g^2; t/a^2)$, we need to determine pairs of $(g^2,\ \beta(g^2))$ at selected flow times for values of g^2 between those that emerge from the ensembles. As in the example of Fig. 3, we interpolate $\beta(g^2; t/a^2)$ with a quadratic form according to $\beta(g^2; t/a^2)/g^4 = c_0 + c_1 g^2 + c_2 g^4$ at a series of flow times. (See Ref. [16] for details.) We do the same for the other flows.[3] The fit function with three free coefficients describes the data well with p-value $p \gtrsim 0.3$. As usual in interpolating data, we will not use the interpolating curves outside the range of the interpolation when taking the continuum limit. The columns labelled $g^2_{\rm min}$ and

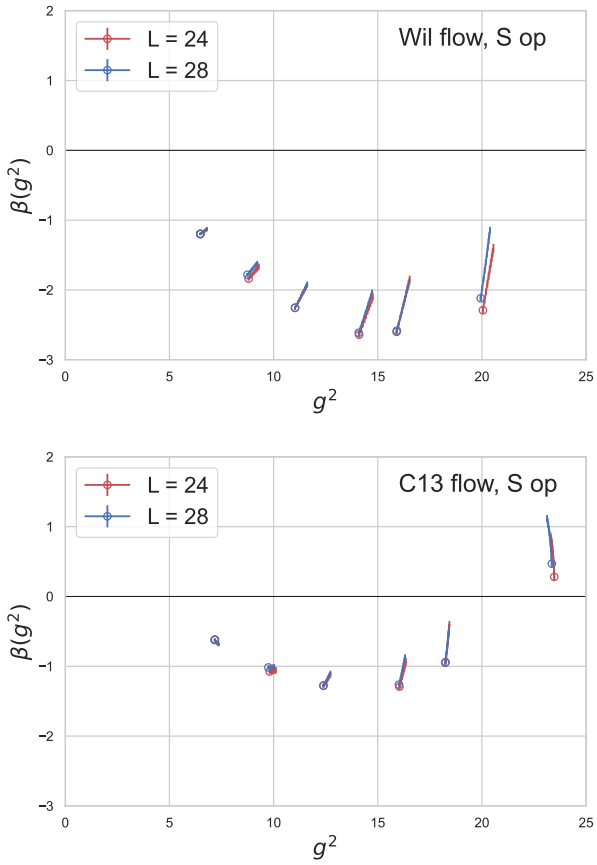

FIG. 2. Raw data for the flowed coupling g^2 and its derivative $\beta(g^2)$, calculated from the Symanzik operator. The upper panel shows results for the Wilson flow; the lower, for C13 flow. Each ensemble is represented by a group of data points: From right to left: $\beta_0 = 6.0$, 6.2, 6.3, 6.5, 6.7, 7.0. In each group, the ensemble average at $t = 2.8$ is plotted as a circle, from which rises the sequence of averages calculated at increasing t for $2.8 < t/a^2 \leq 3.8$, rising as t grows. The lines at each point give a sense for the magnitude and direction of the continuum extrapolation $a^2/t \to 0$. The colors allow comparison of lattice size $L/a = 24$ (red) to $L/a = 28$ (blue).

[2] This volume dependence has been extensively studied and verified in other studies of the continuous β function [8, 18, 27].

[3] The C13 flow shows strong cutoff effects at the weakest bare gauge coupling $\beta_0 = 7.0$, and hence we do not include that value in the interpolation. Similar phenomena were observed and discussed in Ref. [16].

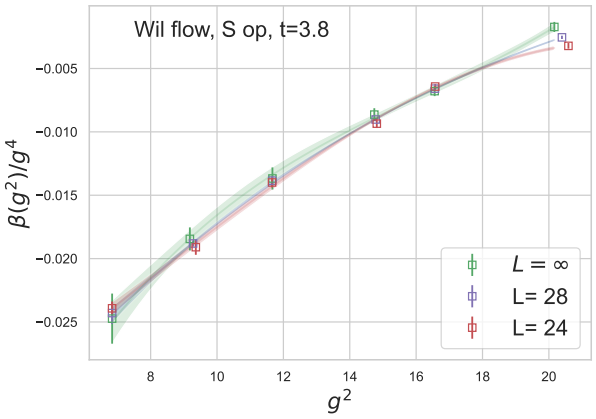

FIG. 3. Comparing the interpolations of $L/a = 24$ (red) and $L/a = 28$ (blue), derived with Wilson flow, S operator at flow time $t/a^2 = 3.8$ (the largest flow time we consider). The green symbols show the extrapolation to infinite volume. The colored bands correspond to quadratic interpolations as explained in Sec. III B.

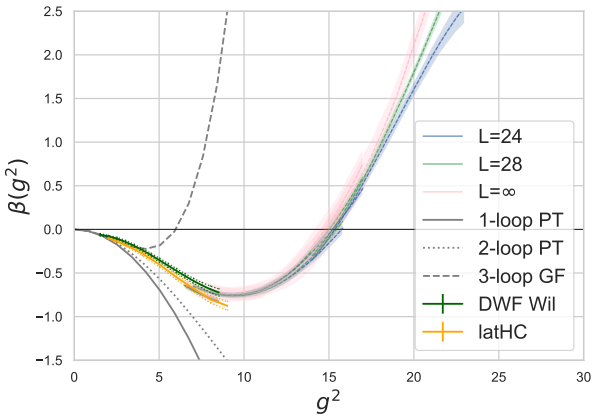

FIG. 4. Same as Fig. 1, but showing the β function obtained by working at fixed lattice volumes $L/a = 24$ (blue) and $L/a = 28$ (green), as well as the infinite volume extrapolation (pink). For simplicity, we do not distinguish among the different gradient flows as we do in Fig. 1.

$g^2_{\rm max1}$ in Table 2 list the minimal and maximal values covered by the interpolating curves.

C. Continuum limit

After determining interpolating curves as in Fig. 3 for many values of t/a^2 in the interval $[2.8, 3.8]$, we extrapolate $\beta(g^2; t/a^2)$ to $t/a^2 = \infty$ at fixed g^2. One such extrapolation is shown in Fig. 5. Repeating this in a range of g^2 gives the β function that is plotted in Fig. 1. We show curves and error bands for the results of Symanzik, Wilson, C23, and C13 flows. These must agree in the continuum limit. Figure 5, in particular, shows the excellent agreement of Wilson and C13 flows at $g^2 = 15.0$, and the fact that $\beta(g^2)$ is consistent with zero there.

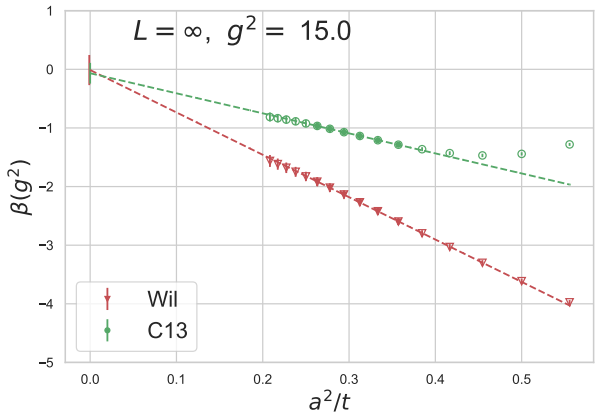

FIG. 5. Continuum extrapolation $a^2/t \to 0$ of the S operator for Wilson and C13 flows at $g^2 = 15.0$ in the infinite-volume limit. The solid symbols correspond to $2.8 \le t/a^2 \le 3.8$, the range of flow time used in the extrapolations. The curvature observed at small t (large a^2/t) indicates that the flow has not yet reached the renormalized trajectory.

It can be seen in Fig. 1 that each flow is plotted in a restricted range of g^2. This stems from a requirement of internal consistency, as follows.

D. Consistency tests

At any given physical coupling g^2, the β functions based on different discretizations of the flowed energy density—the S, W, and C operators—must agree in the continuum limit. For each flow, we use this requirement on the operators to impose cuts on the range of g^2 where that flow can be trusted.

We return to the continuum extrapolation of Fig. 5, but we step back to consider only a single volume (cf. Fig. 3) where we compare the results stemming from the three operators, S, W, and C. We show an example of these continuum extrapolations in Fig. 6. For all flows and at every g^2 we observe that the S operator's extrapolation has the smallest slope, meaning the smallest cutoff effects, with the W operator coming next. The C operator is furthest from the continuum limit, having the largest slopes. This naturally leads to the choice of the S operator for our main result, but we require consistency between the S and W operators. We label the extrapolated values of the S and W data at each value of g^2 as $\beta_{\rm S}$ and $\beta_{\rm W}$.

We base the criterion for consistency on plots like Fig. 7, which is obtained from a bootstrap analysis and includes correlations among the different operators. The green band is the $\pm 1\sigma$ error band of the difference $\beta_{\rm S} - \beta_{\rm W}$. The solid red curves represent $\pm\sqrt{2}\sigma_{\rm S}$, where

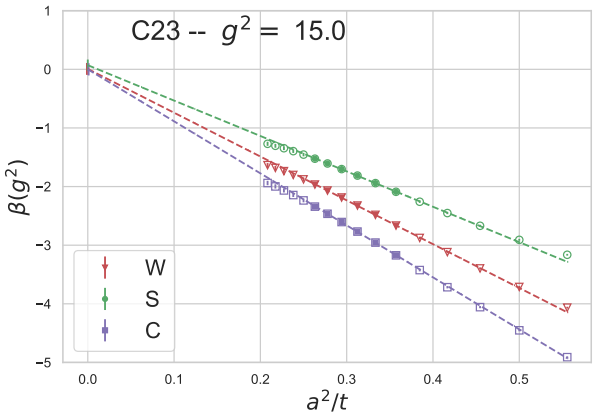

FIG. 6. Continuum limits $a^2/t \to 0$ of data from the C23 flow on the single volume $24^3 \times 48$ (cf. Fig. 5). We show the extrapolation of data from S, W, and C operators. We use the S and W extrapolations to test for consistency. The small curvature observed in the data at large flow times (small a^2/t) indicates finite volume effects, absent from the $L \to \infty$ limit shown in Fig. 5.

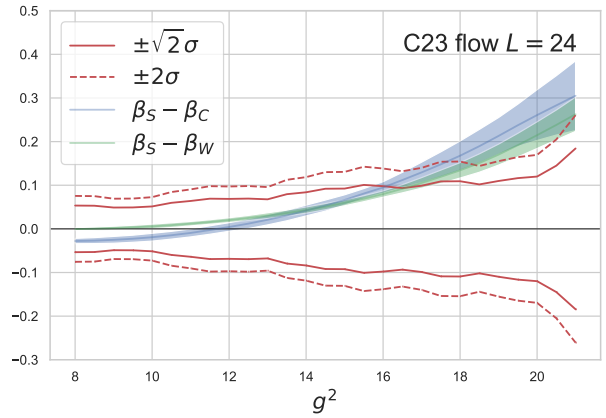

FIG. 7. Comparing the differences $\beta_S - \beta_W$ (green) and $\beta_S - \beta_C$ (blue) with the standard deviation σ of the S operator on volume $24^3 \times 48$ for the C23 flow. We plot $\pm\sqrt{2}\sigma$ (solid red curves) and $\pm 2\sigma$ (dashed red curves). Together with a similar plot for volume $28^3 \times 56$, the crossings of $\beta_S - \beta_W$ with the dashed and solid red curves determine the bounds of validity $g^2_{\rm max2}$ and $g^2_{\rm max3}$ in Table 2.

Flow	$g^2_{\rm min}$	$g^2_{\rm max1}$	$g^2_{\rm max2}$	$g^2_{\rm max3}$
Sym	6.5	18.0	8.5	7.5
Wil	7.0	20.0	16.0	10.0
C23	8.0	21.0	18.0	16.0
C13	12.0	23.0	23.0	21.0

TABLE 2. Ranges of g^2 in which each flow is included in the final result for $\beta(g^2)$. $g^2_{\rm min}$ and $g^2_{\rm max1}$ result from the interpolations, while $g^2_{\rm max2}$ and $g^2_{\rm max3}$ come from further demanding consistency between the continuum extrapolations $\beta_{\rm S}$ and $\beta_{\rm W}$ (see Fig. 7). We quote all numbers with a resolution of 0.5. $g^2_{\rm min}$ and $g^2_{\rm max2}$ give the ranges reflected in Fig. 1. $g^2_{\rm max3}$, rather than $g^2_{\rm max2}$, gives the stricter bounds shown in Fig. 8.

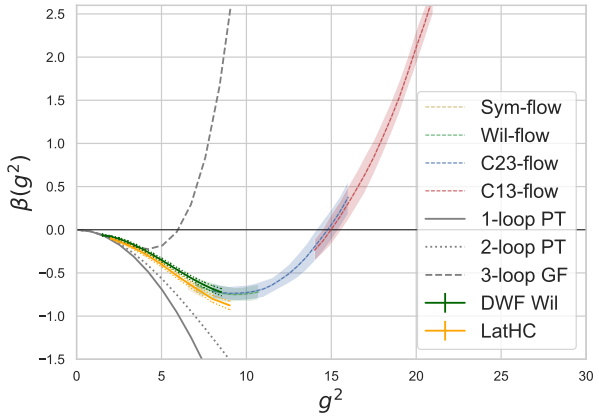

FIG. 8. Same as Fig. 1, but with stricter bounds on the domain of validity of each flow. See Table 2.

$\sigma_{\rm S}$ is the error in $\beta_{\rm S}$, while the dashed red curves are $\pm 2\sigma_{\rm S}$. The green band is much narrower than the span between the red curves; this reflects the strong correlations between the operators. For a consistency test we require $|\beta_{\rm S} - \beta_{\rm W}| \lesssim 2\sigma_S$ on $L = 24$ and 28 volumes separately and simultaneously. This requirement restricts the g^2 values where a given flow can be trusted. Table 2 lists the corresponding values for each flow. The demand that $|\beta_{\rm S} - \beta_{\rm W}| \lesssim 2\sigma_S$ gives us the bounds for each flow that are listed in columns 2 and 4 in the table and shown in Fig. 1. A slightly stricter constraint is obtained by requiring $|\beta_{\rm S} - \beta_{\rm W}| \lesssim \sqrt{2}\sigma_S$. This lowers some of the upper bounds, as shown in the table (see column 5) and in Fig. 8. In this case the Wilson flow no longer reaches the fixed point, but there is little effect on the C23 and C13 flows, which do.

We have verified that an alternative analysis using C instead of W (also shown in Fig. 7) leads to consistency bounds close to the above.

IV. ANOMALOUS DIMENSIONS

The calculation of anomalous dimensions follows that of Ref. [16] closely, with the addition of an extrapolation to infinite volume as described in Sec. III A above. We calculated the two-point function of each flowed mesonic density X' with its unflowed source X,

$$\langle X(0)\, X'(t)\rangle \sim t^{-(d+\eta+\gamma)/2}\,. \tag{4.1}$$

Here γ is the desired anomalous dimension of the operator and $\eta/2$ is the anomalous dimension of the the elementary fermion field. To eliminate η, we divide $\langle X(0)\, X'(t)\rangle$ by the two-point function of the conserved vector current. Defining the ratio

$$R(t) = \frac{\langle X(0)\, X'(t)\rangle}{\langle V(0)\, V'(t)\rangle}\,, \tag{4.2}$$

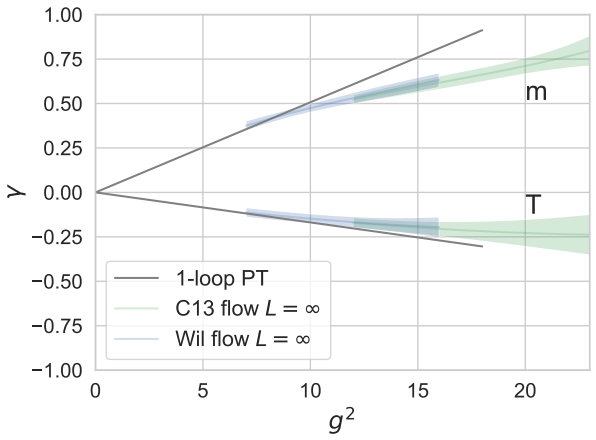

FIG. 9. The anomalous dimension of the mass (scalar) operator, γ_m, and that of the tensor operator, γ_T, obtained with Wilson and C13 flows, extrapolated to the continuum limit and to infinite volume.

we have

$$R(t) \sim t^{-\gamma/2} \ , \tag{4.3}$$

and hence γ can be extracted from the logarithmic derivative,

$$\gamma = -2\frac{t}{R}\frac{\partial R}{\partial t} \ . \tag{4.4}$$

We require $\sqrt{8t} \ll x_4$, where x_4 is the separation of X and X' in Euclidean time. This means that x_4 is kept large compared to the smearing of the operators by the flow. The extrapolation from $L/a = 24, 28$ to $L = \infty$, the interpolation in g^2 at fixed t, and the continuum extrapolation $t/a^2 \to \infty$ are as described above and in Ref. [16].

Final results for the mass anomalous dimension and for that of the tensor density are shown in Fig. 9. In the weak-coupling region, the anomalous dimensions agree with one-loop perturbation theory,

$$\gamma_m = \frac{6g^2C_2}{16\pi^2} \ , \quad \gamma_T = -\frac{1}{3}\gamma_m \ , \tag{4.5}$$

where $C_2 = 4/3$ is the quadratic Casimir operator of the fermion representation. At larger couplings, the magnitudes of both γ_m and γ_T drop below the respective one-loop results. At the IR fixed point $g^2 \simeq 15$ we find $\gamma_m \simeq 0.6$ and $\gamma_T \simeq -0.2$.

The LSD collaboration [29, 30] calculated γ_m in the 4+6 mass-split system using hyperscaling relations and reported $\gamma_m = 0.47(5)$. That work performed simulations near $g^2 \simeq 10$. Accounting for the dependence of γ_m on g^2 (cf. Fig. 9), the two values are consistent.

V. CONCLUSIONS

We have presented a calculation of the β function of the SU(3) gauge theory with $N_f = 10$. We have used Pauli–Villars bosons to improve the gauge action [14] and new techniques pioneered in [16] to combine multiple lattice gradient flows. Our result is represented by a consistent set of curves that derive from gradient-flow transformations with overlapping regions of validity, giving overall a smooth graph of the β function. Our work makes contact with existing results at weak coupling and reaches much larger couplings than previously attainable.

We obtain strong evidence for an infrared-stable fixed point at $g^2 \simeq 15$, whose location is consistently identified by three different flows. This places the theory inside the conformal window for SU(3) gauge theories with fermions in the fundamental representation. We remind the reader that the Banks-Zaks fixed point [31], based on the two-loop β function, places the sill of the window at $N_f = 8.05$.

We have similarly calculated the anomalous dimensions γ_m and γ_T. As shown above, the mass anomalous dimension has the value $\gamma_m \simeq 0.6$ at the fixed point, in good agreement with the value of 0.615 obtained by Ryttov and Shrock using their scheme-independent series expansion to fourth order [32, 33]. Likewise, there is good agreement for the tensor anomalous dimension, for which they obtained the value of -0.149 at third order [34].

It is generally expected [35] that $\gamma_m \to 1$ at the sill of the conformal window. Our result suggests that the $N_f = 10$ theory is well above the sill.

ACKNOWLEDGMENTS

We thank R. Shrock for correspondence about Refs. [32–34]. Computations for this work were carried out on facilities of the USQCD Collaboration, which are funded by the Office of Science of the U.S. Department of Energy. A.H. and E.N. acknowledge support by DOE grant DE-SC0010005. The work of B.S. and Y.S. was supported by the Israel Science Foundation under grant No. 1429/21. Our simulation code is a derivative of the MILC code [36].

[1] T.-W. Chiu, The β-function of $SU(3)$ gauge theory with $N_f = 10$ massless fermions in the fundamental representation, (2016), arXiv:1603.08854 [hep-lat].

[2] T.-W. Chiu, Discrete β-function of the $SU(3)$ gauge theory with 10 massless domain-wall fermions, PoS **LATTICE2016**, 228 (2017).

[3] T.-W. Chiu, Improved study of the β-function of $SU(3)$ gauge theory with $N_f = 10$ massless domain-wall fermions, Phys. Rev. D **99**, 014507 (2019), arXiv:1811.01729 [hep-lat].

[4] A. Hasenfratz, C. Rebbi, and O. Witzel, Nonperturbative determination of β functions for SU(3) gauge theories with 10 and 12 fundamental flavors using domain wall fermions, Phys. Lett. **B798**, 134937 (2019), arXiv:1710.11578 [hep-lat].

[5] A. Hasenfratz, C. Rebbi, and O. Witzel, Gradient flow step-scaling function for SU(3) with ten fundamental flavors, Phys. Rev. D **101**, 114508 (2020), arXiv:2004.00754 [hep-lat].

[6] Z. Fodor, K. Holland, J. Kuti, D. Nogradi, and C. H. Wong, Fate of a recent conformal fixed point and β-function in the SU(3) BSM gauge theory with ten massless flavors, PoS **LATTICE2018**, 199 (2018), arXiv:1812.03972 [hep-lat].

[7] Z. Fodor, K. Holland, J. Kuti, D. Nogradi, and C. H. Wong, Case studies of near-conformal β-functions, PoS **LATTICE2019**, 121 (2019), arXiv:1912.07653 [hep-lat].

[8] J. Kuti, Z. Fodor, K. Holland, and C. H. Wong, From ten-flavor tests of the β-function to α_s at the Z-pole, PoS **LATTICE2021**, 321 (2022), arXiv:2203.15847 [hep-lat].

[9] M. Lüscher, Properties and uses of the Wilson flow in lattice QCD, JHEP **08**, 071, [Erratum: JHEP 03, 092 (2014)], arXiv:1006.4518 [hep-lat].

[10] M. Lüscher, Chiral symmetry and the Yang–Mills gradient flow, JHEP **04**, 123, arXiv:1302.5246 [hep-lat].

[11] Z. Fodor, K. Holland, J. Kuti, D. Nogradi, and C. H. Wong, The Yang-Mills gradient flow in finite volume, JHEP **11**, 007, arXiv:1208.1051 [hep-lat].

[12] A. Hasenfratz and O. Witzel, Continuous β function for SU(3) with N_f fundamental flavors, work in progress (2023).

[13] R. V. Harlander and T. Neumann, The perturbative QCD gradient flow to three loops, JHEP **06**, 161, arXiv:1606.03756 [hep-ph].

[14] A. Hasenfratz, Y. Shamir, and B. Svetitsky, Taming lattice artifacts with Pauli-Villars fields, Phys. Rev. D **104**, 074509 (2021), arXiv:2109.02790 [hep-lat].

[15] A. Hasenfratz, Emergent strongly coupled ultraviolet fixed point in four dimensions with eight Kähler-Dirac fermions, Phys. Rev. D **106**, 014513 (2022), arXiv:2204.04801 [hep-lat].

[16] A. Hasenfratz, E. T. Neil, Y. Shamir, B. Svetitsky, and O. Witzel, Infrared fixed point and anomalous dimensions in a composite Higgs model, (2023), arXiv:2304.11729 [hep-lat].

[17] A. Hasenfratz and O. Witzel, Continuous renormalization group β function from lattice simulations, Phys. Rev. D **101**, 034514 (2020), arXiv:1910.06408 [hep-lat].

[18] A. Hasenfratz and O. Witzel, Continuous β function for the SU(3) gauge systems with two and twelve fundamental flavors, PoS **LATTICE2019**, 094 (2019), arXiv:1911.11531 [hep-lat].

[19] A. Hasenfratz and F. Knechtli, Flavor symmetry and the static potential with hypercubic blocking, Phys. Rev. **D64**, 034504 (2001), arXiv:hep-lat/0103029 [hep-lat].

[20] A. Hasenfratz, R. Hoffmann, and S. Schaefer, Hypercubic smeared links for dynamical fermions, JHEP **05**, 029, arXiv:hep-lat/0702028 [hep-lat].

[21] C. W. Bernard and T. A. DeGrand, Perturbation theory for fat link fermion actions, *Lattice field theory. Proceedings, 17th International Symposium, Lattice'99, Pisa, Italy, June 29-July 3, 1999*, Nucl. Phys. Proc. Suppl. **83**, 845 (2000), arXiv:hep-lat/9909083 [hep-lat].

[22] Y. Shamir, B. Svetitsky, and E. Yurkovsky, Improvement via hypercubic smearing in triplet and sextet QCD, Phys. Rev. D **83**, 097502 (2011), arXiv:1012.2819 [hep-lat].

[23] T. DeGrand, Y. Shamir, and B. Svetitsky, Suppressing dislocations in normalized hypercubic smearing, Phys. Rev. **D90**, 054501 (2014), arXiv:1407.4201 [hep-lat].

[24] A. Carosso, A. Hasenfratz, and E. T. Neil, Nonperturbative Renormalization of Operators in Near-Conformal Systems Using Gradient Flows, Phys. Rev. Lett. **121**, 201601 (2018), arXiv:1806.01385 [hep-lat].

[25] Z. Fodor, K. Holland, J. Kuti, D. Nogradi, and C. H. Wong, A new method for the beta function in the chiral symmetry broken phase, EPJ Web Conf. **175**, 08027 (2018), arXiv:1711.04833 [hep-lat].

[26] C. T. Peterson, A. Hasenfratz, J. van Sickle, and O. Witzel, Determination of the continuous β function of SU(3) Yang-Mills theory, PoS **LATTICE2021**, 174 (2022), arXiv:2109.09720 [hep-lat].

[27] A. Hasenfratz, C. T. Peterson, J. van Sickle, and O. Witzel, Λ parameter of the SU(3) Yang-Mills theory from the continuous β function, (2023), arXiv:2303.00704 [hep-lat].

[28] A. Hasenfratz, C. J. Monahan, M. D. Rizik, A. Shindler, and O. Witzel, A novel nonperturbative renormalization scheme for local operators, PoS **LATTICE2021**, 155 (2022), arXiv:2201.09740 [hep-lat].

[29] T. Appelquist *et al.* (Lattice Strong Dynamics), Near-conformal dynamics in a chirally broken system, Phys. Rev. D **103**, 014504 (2021), arXiv:2007.01810 [hep-ph].

[30] O. Witzel, A. Hasenfratz, and C. T. Peterson (Lattice Strong Dynamics), Composite Higgs scenario in mass-split models, PoS **ICHEP2020**, 675 (2021), arXiv:2011.05175 [hep-ph].

[31] T. Banks and A. Zaks, On the Phase Structure of Vector-Like Gauge Theories with Massless Fermions, Nucl. Phys. B **196**, 189 (1982).

[32] T. A. Ryttov and R. Shrock, Scheme-independent calculation of $\gamma_{\bar{\psi}\psi,IR}$ for an SU(3) gauge theory, Phys. Rev. D **94**, 105014 (2016), arXiv:1608.00068 [hep-th].

[33] T. A. Ryttov and R. Shrock, Higher-order scheme-independent series expansions of $\gamma_{\bar{\psi}\psi,IR}$ and β'_{IR} in conformal field theories, Phys. Rev. D **95**, 105004 (2017), arXiv:1703.08558 [hep-th].

[34] T. A. Ryttov and R. Shrock, Scheme-Independent Series Expansions at an Infrared Zero of the Beta Function in Asymptotically Free Gauge Theories, Phys. Rev. D **94**, 125005 (2016), arXiv:1610.00387 [hep-th].

[35] B. S. Kim, D. K. Hong, and J.-W. Lee, Into the conformal window: Multirepresentation gauge theories, Phys. Rev. D **101**, 056008 (2020), arXiv:2001.02690 [hep-ph].

[36] MILC Collaboration, `http://www.physics.utah.edu/~detar/milc/`.